Correlation gap in the heavy-fermion antiferromagnet UPd_2Al_3

M. Dressel[*], N. Kasper[‡], K. Petukhov, D.N. Peligrad, and B. Gorshunov[†]

Physikalisches Institut, Universität Stuttgart, Pfaffenwaldring 57, D-70550 Stuttgart, Germany

M. Jourdan, M. Huth, and H. Adrian

Institut für Physik, Universität Mainz, Staudinger Weg 7, D-55099 Mainz, Germany

The optical properties of the heavy-fermion compound UPd_2Al_3 have been measured in the frequency range from 0.04 meV to 5 meV (0.3 to 40 cm^{-1}) at temperatures 2 K < T < 300 K. Below the coherence temperature $T^* \approx 50$ K, the hybridization gap opens around 10 meV. As the temperature decreases further ($T \leq 20$ K), a well pronounced pseudogap of approximately 0.2 meV develops in the optical response; we relate this to the antiferromagnetic ordering which occurs below $T_N \approx 14$ K. The frequency dependent mass and scattering rate give evidence that the enhancement of the effective mass mainly occurs below the energy which is associated to the magnetic correlations between the itinerant and localized $5f$ electrons. In addition to this correlation gap, we observe a narrow zero-frequency conductivity peak which at 2 K is less than 0.1 meV wide, and which contains only a fraction of the delocalized carriers. The analysis of the spectral weight infers a loss of kinetic energy associated with the superconducting transition.

I. INTRODUCTION

More than twenty years after the discovery of superconductivity in heavy-fermion (HF) compounds,[1] the nature of the superconducting ground state is still under debate. In particular the discovery of the coexistence of antiferromagnetic (AF) ordering and superconductivity in some of these materials has reinforced the interest to study the interplay between electronic and magnetic degrees of freedom in these correlated electron systems. Instead of the conventional electron-phonon interaction, the electron-magnon correlations have been proposed to cause the pairing in HF superconductors.[2,3] Heavy fermions are intermetallic compounds containing elements with f electrons which show a large enhancement of the quasiparticle effective mass. The wavefunctions of the atomic and conduction electrons mix (hybridization), and the strong interaction of the quasi-free conduction-band electrons with nearly localized f electrons leads to a so-called Abrikosov-Suhl resonance, i.e. an enhanced density of states at the Fermi energy.[3] The main idea of understanding this state of matter is the competition between Kondo and Ruderman-Kittel-Kasuya-Yosida (RKKY) interactions. The RKKY interaction leads to a magnetic ground state while the dominance of the Kondo interaction causes hybridization between localized f-electron states and delocalized conduction electrons. Due to the arrangement of the f orbitals on a regular lattice, the hybridization with the itinerant states leads to the opening of a charge gap at the Fermi energy; hence if not fully developed at least a pseudogap should show up in the electronic excitation spectrum.[4–8]

The common feature of the HF systems is the crossover from an incoherent state, where the scattering of the charge carriers on magnetic moments can be described in the frame of the single-particle Kondo model, to a many-body ground state (Kondo lattice) on cooling below the coherence temperature T^*. Above T^* the optical conductivity exhibits a broad Drude behavior

$$\hat{\sigma}(\omega) = \sigma_1(\omega) + i\sigma_2(\omega) = \frac{\sigma_{dc}}{1 + i\omega\tau} \qquad (1)$$

which characterizes normal metals;[9] the dc conductivity is given by $\sigma_{dc} = ne^2\tau/m$ with n the concentration of conduction electrons, e and m the electronic charge and mass, and $1/\tau = \Gamma$ the scattering rate, which is typically a few hundred wavenumbers for usual metals. The area under the conductivity spectrum is the spectral weight:

$$\int \sigma_1(\omega)\, d\omega = \frac{\pi n e^2}{2m} = \frac{\omega_p^2}{8} \qquad (2)$$

and determines the plasma frequency $\omega_p = \sqrt{4\pi n e^2/m}$.

Below the coherence temperature T^*, however, the increase in the density of electronic states (DOS) at low energies is commonly described by the formation of a narrow Drude peak with a renormalized effective mass m^* and scattering rate Γ^* of charge carriers:[10–12]

$$\hat{\sigma}(\omega) = \frac{(\omega_p^*)^2}{4\pi} \frac{1}{\Gamma^* + i\omega}. \qquad (3)$$

Because $m^*\Gamma^* = m\Gamma$, the dc conductivity $\sigma_{dc} = ne^2/(m^*\Gamma^*)$ is not affected by the renormalization. The spectral weight $\omega_p^{*2}/8 = \pi ne^2/(2m^*)$, however, decreases as m^* increases; typically m^* can reach several hundred times the free electron mass m. The enhancement of the effective mass is connected to the hybridization of s and f-orbitals which leads to a narrow band with a high DOS at the Fermi energy and to the strong coupling of

the charge carriers to the local magnetic moments.[10,11] In HF compounds which do not order magnetically, a scaling relation

$$\left(\frac{\Delta}{T^*}\right)^2 = \frac{m^*}{m} \qquad (4)$$

between the hybridization gap Δ and the enhancement of the effective mass m^*/m is found theoretically[4−8] and experimentally.[13−15] With T^* in the order of 10 to 100 K the hybridization gap is normally observed in the far-infrared range of frequency.

The antiferromagnetic ordering reveals itself in rather different ways for the various HF compounds.[12,16] For instance, UPt$_3$ does not show[17,18] any appreciable anomaly of the specific heat or resistivity at the Néel temperature $T_N = 5$ K while in URu$_2$Si$_2$ and UPd$_2$Al$_3$ the transition into a magnetically ordered state is accompanied by clear anomalies of these quantities.[19,20] However, URu$_2$Si$_2$ shows a remarkable resistivity increase at T_N, typical for a spin-density-wave (SDW) system, while in UPd$_2$Al$_3$ only a kink in the $\rho(T)$ due to freezing-out of the spin-flip-scattering is observed.[16] This already indicates that in contrast to the former system with itinerant antiferromagnetism, UPd$_2$Al$_3$ is an antiferromagnet with localized spins. In both UPt$_3$ and URu$_2$Si$_2$, but also in UCu$_5$, the progressive development of a gap (or pseudo-gap) in the optical spectra is observed in connection with the ordering of the magnetic moments,[16,18,21,22] whereas for UPd$_2$Al$_3$ no effect of magnetic ordering on the optical response at frequencies above 30 cm^{-1} has been detected in the first infrared investigations.[16,23]

In the heavy fermion superconductor UPd$_2$Al$_3$, on which we want to focus in this paper, a maximum of the resistivity occurs at temperaturea around 80 K which is often related to the onset of coherence;[24] the values cited for the coherence temperature T^* range from 20 K to 60 K depending on the experimental method used for determination. The magnetic susceptibility $\chi(T)$ shows appreciably different behaviors for field directions parallel and perpendicular to the hexagonal c-axis;[25] in the ab-plane $\chi(T)$ is Curie-Weiss like above 40 K with a maximum at around 35 K. Below this temperature, AF correlations develop, and UPd$_2$Al$_3$ shows a metamagnetic behavior. When cooling down even further, a commensurate AF order develops below $T_N = 14$ K; superconductivity finally sets in[20,26,27] below 2 K. For 2 K $< T <$ 14 K the specific heat shows a $C/T \propto T^2$ dependence; the effective mass of the charge carriers is estimated[20,28] as $m^*/m \approx 50$.

In the superconducting state of UPd$_2$Al$_3$ two low-energy modes at 1.5 meV and 0.4 meV have been observed[29] by inelastic neutron scattering experiments at $\mathbf{q} = \frac{1}{2c}(0,0,1)$; it was suggested that they are associated with magnetic excitons and superconductivity, respectively. An important feature of UPd$_2$Al$_3$ is that – compared with other HF antiferromagnets – it has a rather large magnetic moment (0.85 μ_B) which is localized predominantly on the U-site.[26,30] Based on this ex-

perimental evidence, it has been suggested that UPd$_2$Al$_3$ can be described as a local-moment magnet, and hence the magnetic ordering should have only a minor influence on the electronic DOS. However, theoretical calculations of the Fermi surface[31] as well as de Haas-van Alphen experiments[32] also indicate an itinerant character of 5f-electrons, and therefore one can expect in UPd$_2$Al$_3$ to find appreciable correlations between electronic states and magnetic ordering. Besides the interesting interplay of magnetic ordering and superconductivity, these correlations make UPd$_2$Al$_3$ one of the most studied HF systems in recent years; they are the main subject of our investigation.

Optical experiments have in general proven to be sensitive to the formation of heavy quasiparticles;[11,12] the relevant features show up at the lower end of the infrared spectral range which is commonly accessible. In order to extend our earlier investigations[16,23] to lower frequencies, in the present work we have carried out optical experiments on UPd$_2$Al$_3$ films in the spectral range from microwaves up to the far infrared. First results have partially been reported in Refs. 33–35.

II. EXPERIMENTAL METHODS

The highly c-axis oriented, epitaxial thin (150 nm) film of UPd$_2$Al$_3$ was prepared on (111) oriented LaAlO$_3$ substrate (thickness 0.924 mm) by electron-beam co-evaporation of the constituent elements in a molecular-beam epitaxy system.[36] The phase purity and structure of the film were investigated by X-ray and reflection high-energy electron diffraction. The high quality of the film is seen in dc resistivity data displayed in Fig. 1 which are in excellent agreement with measurements of bulk crystals.[20] At $T = 300$ K the resistivity is $\rho = 172$ $\mu\Omega$cm, the residual resistivity ratio $\rho_{300K}/\rho_{2K} = 23$, the Néel temperature $T_N = 14$ K; our film shows a sharp superconducting transition at $T_c = 1.75$ K.

For the measurements in the millimeter and sub-millimeter spectral range (50 − 1400 GHz, 1.2 − 40 cm^{-1}, 0.2 − 5 meV) a coherent source spectrometer was employed[37] utilizing a set of different backward wave oscillators as monochromatic and continuously tunable sources. The spectrometer includes an interferometric setup in a Mach-Zehnder arrangement which allows for measuring both the amplitude T_F and the phase ϕ_t of the signal transmitted through the plane-parallel sample, which in our case is a film on a substrate. These two quantities are used to evaluate the complex refractive index $\hat{N} = n + ik$ [or alternatively the complex conductivity $\hat{\sigma}(\omega)$] of the film using Fresnel's formulas for a two-layer system[9] without assuming any particular model. In general, the complex transmission coefficient $\hat{t}_{1234} = \sqrt{T_F}\, e^{i\phi_t}$ of a two-layer system (layers which we index with 2 and 3) separating two media (indices 1 and 4) is given by

$$\hat{t}_{1234} = \hat{t}_{12}\hat{t}_{23}\hat{t}_{34} \exp\{i(\delta_2 + \delta_3)\} \left[1 + \hat{r}_{12}\hat{r}_{23}\exp\{2i\delta_2\}\right.$$
$$\left. +\hat{r}_{23}\hat{r}_{34}\exp\{2i\delta_3\} + \hat{r}_{12}\hat{r}_{34}\exp\{2i(\delta_2+\delta_3)\}\right]^{-1} \quad (5)$$

where the complex angles are $\delta_2 = \omega d_2(n_2 + ik_2)/c$ for the film and $\delta_3 = \omega d_3(n_3 + ik_3)/c$ for the substrate; $c = 3.0 \cdot 10^{10}$ cm/s is the velocity of light in vacuum. The transmission coefficients at each interface are evaluated by the standard equation $\hat{t}_{ij} = (\hat{N}_i - \hat{N}_j)(\hat{N}_i + \hat{N}_j)^{-1}$; where $\hat{N}_1 = \hat{N}_4 = 1$ correspond to vacuum. The optical parameters of the LaAlO$_3$ substrate (n_3 and k_3) are determined beforehand by performing the experiments on a blank substrate. The large size of the sample (approximately 10×10 mm^2) allowed us to extend the measurements to very low frequencies, from $\omega/(2\pi c) = 40$ cm^{-1} down to 1.15 cm^{-1}.

For the infrared range and higher frequencies we used the reflectivity results obtained on bulk samples and published previously.[16,23]

In addition, at the frequencies of 10, 24, and 34 GHz enclosed resonators were developed and the sample was measured by cavity perturbation technique.[38–41] The cylindrical TE$_{011}$ copper cavities – quality factors around $15\,000$ – were operated by Gunn diode oscillators with sufficient tuning range; two waveguides couple to the cavity by holes on the half height of the opposite side walls. A small slice of a sample (typically 3×3 mm^2) was placed in the electrical field maximum. The transmitted power was detected by a diode, amplified and processed by fitting a Lorentzian in order to determine the central frequency f_0 and the width Γ_0. From the shift in frequency Δf and change in width $\Delta\Gamma$ upon introduction of the sample, the surface resistance R_S and the surface reactance X_S which determine the surface impedance $\hat{Z}_S = R_S + iX_S$ are calculated as follows:

$$R_S = Z_0\frac{\Delta\Gamma}{2f_0\zeta} \quad \text{and} \quad X_S = Z_0\frac{\Delta f}{f_0\zeta}, \quad (6)$$

where $Z_0 = 4\pi/c = 4.19 \cdot 10^{-10}$ s/cm is the impedance of free space ($Z_0 = 377\ \Omega$ in SI units). The resonator constant ζ can be calculated from the geometry of the cavity and the sample when the dielectric properties of the substrate are known.[38,41] The complex conductivity $\hat{\sigma}$ can be evaluated from the surface impedance using $\hat{Z}_S = Z_0\sqrt{\omega/4\pi i\hat{\sigma}}$, and the absorptivity A (sometimes simply called the absorption) is given by the relation

$$A = 1 - R = \frac{4R_S}{Z_0}\left(1 + \frac{2R_S}{Z_0} + \frac{R_S^2 + X_S^2}{Z_0^2}\right)^{-1}, \quad (7)$$

where R is the reflectivity. In the limit $R_S, |X_S| \ll Z_0$, the last equation reduces to

$$A \approx 4R_S/Z_0. \quad (8)$$

While at 10 GHz the two components of the complex surface impedance could be measured and therefore both the conductivity and the dielectric constant were calculated, in our higher frequency experiments at 24 and

34 GHz – because of the large influence of the substrate – we were not able to determine the frequency shift accurately enough to evaluate the dielectric properties of the film; hence we only utilize the surface resistance R_S. By using Eq. (8), however, it was possible to combine these millimeter wave cavity data with all of the higher frequency optical data, i.e. the transmission results through the films obtained in the submillimeter wave range and the reflectivity[16,23] measured on bulk samples in the infrared, visible and ultraviolet spectral range. The reflection coefficient is a complex function $\hat{r}(\omega) = |r(\omega)|e^{i\phi_r(\omega)}$ with the measured bulk reflectivity $R = |\hat{r}|^2$. In order to obtain the phase ϕ_r we performed a Kramers-Kronig analysis on the reflectivity spectra:[9]

$$\phi_r(\omega) = \frac{\omega}{\pi}\int_0^\infty \frac{\ln[R(\omega')] - \ln[R(\omega)]}{\omega^2 - (\omega')^2}\,d\omega', \quad (9)$$

where the $\ln[R(\omega)]$ term has been added to the standard form in order to remove the singularity at $\omega' = \omega$. It has no effect on the integral because $\int_0^\infty[\omega^2 - (\omega')^2]^{-1}d\omega' = 0$. Because this integral extends from zero to infinity, it is necessary to make suitable high and low frequency extrapolations to the measured reflectivity data. We have chosen to use a power law $[R(\omega) \propto 1/\omega^4]$ at high frequencies above 10^6 cm^{-1} and a Hagen-Rubens extrapolation

$$R(\omega) = 1 - \left(\frac{2\omega}{\pi\sigma_{\text{dc}}}\right)^{1/2} \quad (10)$$

below 0.3 cm^{-1}. From $R(\omega)$ and $\phi_r(\omega)$ it is then possible[9] to calculate the complex optical conductivity $\hat{\sigma}(\omega)$.

III. RESULTS AND ANALYSIS

A. Transmission Spectra

In Fig. 2 we present the low-frequency transmission spectra for the UPd$_2$Al$_3$ film on the substrate for two selected temperatures (100 K and 2 K); they already illustrate clearly our main finding. The fringes in the spectra are due to multi-reflection of the radiation within the plane-parallel substrate acting as a Fabry-Perot resonator for our monochromatic radiation.[9] The frequency spacing between two peaks is mainly determined by the thickness and refractive index of the substrate; their amplitude (minima to maxima), however, is governed by the parameters of the film. At temperatures above 25 K, the transmission spectra basically do not change. For $T \leq 20$ K the overall transmission is found to be strongly reduced below 10 cm^{-1} due to absorption within the film. At lower frequencies, $\nu = \omega/(2\pi c) < 3.5$ cm^{-1}, the transmitted signal increases again, indicating an absorption edge. It is worth to note, that our preliminary study of a 136 nm thick UPd$_2$Al$_3$ film showed the same features in the optical response.[33]

3

This feature appears below the temperature where the magnetic susceptibility has a maximum – when the AF correlations develop. Therefore we checked whether the observed transmission minimum could be due to some magnetic absorption. We tried to fit the observed behavior by modelling the complex permeability $\hat{\mu}(\omega)$ with a magnetic oscillator (Lorentzian):

$$\hat{\mu}(\omega) = 1 + \frac{\Delta\mu_1\omega_0^2}{\omega_0^2 - \omega^2 + i\omega\Gamma} \qquad (11)$$

where ω_0 and Γ are the center frequency and the width of the oscillator, respectively, and $\Delta\mu\,\omega_0^2$ denotes the spectral weight. Alternatively we can satisfactorily describe the transmission spectra by using a dielectric oscillator

$$\hat{\epsilon}(\omega) = \epsilon_1(\omega) + i\epsilon_2(\omega) = 1 + \frac{\Delta\epsilon_1\omega_0^2}{\omega_0^2 - \omega^2 + i\omega\Gamma}. \qquad (12)$$

Here $\Delta\epsilon_1\omega_0^2$ describes the oscillator strength (spectral weight), ω_0 and Γ denote the center frequency and the width of the harmonic oscillator. The results of the least-square fit of the transmitted signal using a Drude–Lorentz model in combination with a magnetic or with a dielectric oscillator are shown in the lower two panels of Fig. 2. The parameters of the magnetic oscillator are $\Delta\mu_1 = 1.001$, $\omega_0/(2\pi c) = 5.45$ cm^{-1}, $\Gamma/(2\pi c) = 4.08$ cm^{-1}; and for the dielectric oscillator we used accordingly $\Delta\epsilon_1 = \omega_p^2/\omega_0^2 = 2.14 \cdot 10^5$, $\omega_0/(2\pi c) = 3.86$ cm^{-1}, $\Gamma/(2\pi c) = 2.13$ cm^{-1}. One can immediately see that, no satisfactory fit is possible with a magnetic oscillator term. Second, the $\Delta\mu_1$ value (which denotes the strength of the magnetic contribution) is much higher than expected from the static magnetic susceptibility measurements.[20] Third, the frequency dependence of the transmission is only described satisfactorily using the dielectric model. Thus we conclude that the observed feature is not due to a pure magnetic excitation and proceed with the analysis of our data along the lines of the complex dielectric constant $\hat{\epsilon}(\omega) = \epsilon_1(\omega) + i\epsilon_2(\omega)$, or complex conductivity $\hat{\sigma} = \hat{\epsilon}\,\omega/(4\pi i)$, respectively.

B. Optical Conductivity

To discuss our findings on the temperature and frequency dependent transport in UPd$_2$Al$_3$, let us first turn back to Fig. 1. Below T_N the temperature dependence of the dc resistivity of the film can be described[28,42,43] using the expression for an antiferromagnet with an energy gap E_g':

$$\rho(T) = \rho_0 + aT^2 + bT\left(1 + \frac{2k_BT}{E_g'}\right)\exp\left\{\frac{-E_g'}{k_BT}\right\}. \qquad (13)$$

Here ρ_0 gives the residual resistivity and the second term describes the electron-electron scattering (Fermi liquid). A fit of the dc curve (dotted line in Fig. 1) by Eq. (13)

yields the gap value $E_g' = 1.9$ meV, which corresponds to the one reported in Ref. 28,36,43.

From early tunneling measurements on UPd$_2$Al$_3$ a rather large spin-gap energy up to 12.4 meV was first suggested.[44] Using thin films of this compound, recent tunneling experiments in the superconducting and normal state clearly demonstrate[45] that there remains a reduced DOS at zero-bias up the temperature range of 7 K with a gap value of 1.0 meV while the superconducting gap is at 0.235 meV. The existence of a gap in either the electronic DOS or in the magnon spectrum was opposed by Caspary et al.[46] and on grounds of infrared measurements by Degiorgi et al.[23] In the light of the low-energy measurements presented in this paper, the arguments will be reconsidered below.

The real parts of the low-frequency optical conductivity $\sigma_1(\omega)$ and of the dielectric constant $\epsilon_1(\omega)$ of UPd$_2$Al$_3$ are plotted in Fig. 3 for some temperatures. Except for the dc conductivity on the left axis of the upper frame and the results of the microwave impedance measurements at 0.3 cm^{-1}, all the data points plotted are obtained directly from the transmitted power and phase shift in our transmission experiments. Within our accuracy both quantities are frequency independent for $T \geq 25$ K, but show a strong dispersion for lower temperatures. In addition, the response of the Drude model [Eq. (3)] is shown (solid line) which matches the dc conductivity $\sigma_{dc} = 1.28 \cdot 10^5$ (Ωcm)$^{-1}$ at 2 K and the far-infrared roll-off around 10 cm^{-1}; it is obvious that the observed optical response of UPd$_2$Al$_3$ differs from that of a renormalized Drude metal. As a result, the simple Hagen-Rubens extrapolation – in general used[12] to extrapolate the far-infrared reflectivity below 30 cm^{-1} – totally misses the following two features in our millimeter and sub-millimeter range. First, the optical conductivity $\sigma_1(\omega)$ clearly shows the development of a gap-like minimum below 3 cm^{-1} at $T < 20$ K; it corresponds to a pronounced increase of the dielectric constant $\epsilon_1(\omega)$ which is a direct measure of the gap. This feature gradually disappears with increasing temperature and is not seen above 30 K. Second, at frequencies below approximately 1.5 cm^{-1} the conductivity increases for $\omega \to 0$ towards considerably higher dc values leading to a very narrow peak at zero frequency.

In a first approach we describe the narrow peak at $\omega = 0$ by the Drude model and use a phenomenological gap model[9,47] for the higher frequencies:

$$\sigma_1(\omega) = \frac{\sigma_{dc}(\Gamma_D^*)^2}{\omega^2 + (\Gamma_D^*)^2} + (1 - \Theta)\frac{\Sigma_g}{\omega^2 + \Gamma_g^2}\sqrt{\omega - \omega_g} \qquad (14)$$

where $\Theta = 1$ for $\omega \leq \omega_g$ and $\Theta = 0$ above the gap frequency ω_g. Here Γ_D^* is the damping of the narrow $\omega = 0$ mode and $E_g = \hbar\omega_g$ corresponds to the gap energy. The parameters Σ_g and Γ_g depend on the concentration, the effective mass, and the scattering rate of the charge carriers above the gap. By performing a Kramers-Kronig integration of Eq. (14) we have also obtained an analyti-

cal expression for the dielectric constant which was used in the fitting procedures. The assumed model (14) describes very well the experimental results of $\sigma_1(\omega)$ and $\epsilon_1(\omega)$ for temperatures $T \leq 20$ K; as an example, the fit of the 2 K data is shown in Fig. 4. The temperature dependence of the gap energy $\hbar\omega_g$ as obtained by this fit is displayed in the inset (solid squares corresponding to the left axis). The gap value $E_g \approx 0.22$ meV is essentially temperature independent, which does not correspond to the well-known BCS-like temperature behavior obtained by mean-field theory; instead, the gap feature becomes more and more pronounced as the temperature is lowered.

While the above analysis was solely based on direct measurements of the optical conductivity and dielectric constant without applying the Kramers-Kronig analysis, we now want to combine all the absorption data available in the entire range of frequency. In Fig. 5a the frequency dependence of the absorptivity $A(\omega) = 1 - R(\omega)$ is plotted over a wide spectral range and for different temperatures. From the measured dc conductivity the absorptivity is calculated in the Hagen-Rubens limit assuming Eq. (10). The full symbols are the results of the microwave cavity measurements of the surface resistance R_S, using Eq. (8). In the range from 1 cm^{-1} to 40 cm^{-1}, the absorptivity is evaluated from our optical experiments using the transmission coefficient and the phase shift (open circles; only 2 K data are plotted for clarity reasons). Above 30 cm^{-1} up to 10^6 cm^{-1} we also utilized the data from bulk reflectivity measurements (solid lines) published previously.[16,23] For even higher frequencies we extrapolated by $R(\omega) \propto \omega^{-4}$. The lines represent the input we used for performing the Kramers-Kronig analysis in order to calculate the optical conductivity. It was obtained by simultaneously fitting the absorptivity results and the directly measured conductivity. Obviously, the low-temperature data exhibit significant deviations from the $A(\omega) \propto \omega^{1/2}$ Hagen-Rubens behavior for frequency above 0.1 cm^{-1}.

The lower panel of Fig. 5 shows the corresponding optical conductivity $\sigma_1(\omega)$ as obtained by a Kramers-Kronig analysis of the absorptivity just described; in addition we again display the directly measured conductivity data which were also taken into account for the absorptivity fit, as mentioned above. The agreement is very good considering the error bars for each measurement technique. The main features can be summarized as follows: (i) At high temperatures $T > 50$ K, we observe a broad conductivity spectrum as expected for a metal according to Eq. (1). Following Ref. 23, the plasma frequency from the evaluation of the entire spectral weight of all free charge carriers is $\omega_p/(2\pi c) = 4.4 \cdot 10^4$ cm^{-1}. (ii) As the temperature decreases below T^*, a renormalized Drude peak [Eq. (3)] develops due to the gradual enhancement of the effective mass m^*. The renormalized plasma frequency $\omega_p^*/(2\pi c) \approx 4350$ cm^{-1}, which will be obtained by the procedure discussed in Subsection III C, corresponds to $m^* \approx 100m$. This behavior is typical for

heavy fermions[12] and was discussed in detail by Degiorgi, Dressel and coworkers[16,23,33,34] for the case of UPd$_2$Al$_3$. At the same time, a gap-like feature develops around 100 cm^{-1} as expected from the hybridization of the localized $5f$ electrons and the conduction electrons; this value is in good agreement with the scaling relation (4). (iii) Lowering the temperature further, magnetic ordering sets in at $T_N = 14$ K and leads to distinct signatures in the optical spectrum. We observe a well pronounced pseudogap below 2 cm^{-1} which we assign to magnetic correlations between the localized and delocalized charge carriers. At even lower frequencies, an extremely narrow mode centered zero-frequency remains which is eventually responsible for superconductivity below $T_c = 2$ K. The analysis and understanding of this low-temperature ($T_c < T \leq T_N$) and low-frequency ($\nu < 50$ cm^{-1}) behavior is the main point of this paper.

For the analysis of our low-frequency data we introduce a complex frequency dependent scattering rate $\hat{\Gamma}(\omega) = \Gamma_1(\omega) + i\Gamma_2(\omega)$ into the standard Drude form of Eq. (3). If we define the dimensionless quantity $\lambda(\omega) = -\Gamma_2(\omega)/\omega$, the complex conductivity can be written as

$$\hat{\sigma}(\omega) = \frac{(\omega_p')^2}{4\pi} \frac{1}{\Gamma_1(\omega) - i\omega(m^*(\omega)/m)} \qquad (15)$$

where $m^*/m = 1 + \lambda(\omega)$ is the frequency dependent enhanced mass. $\omega_p'/(2\pi c) = 9.5 \cdot 10^3$ cm^{-1} corresponds to the fraction of electrons which participate in the many body state which develops below T^* as discussed in the following subsection. By rearranging Eq. (15) we can write expressions for $\Gamma_1(\omega)$ and $m^*(\omega)$ in terms of $\sigma_1(\omega)$ and $\sigma_2(\omega)$ as follows:

$$\Gamma_1(\omega) = \frac{(\omega_p')^2}{4\pi} \frac{\sigma_1(\omega)}{|\hat{\sigma}(\omega)|^2} \qquad (16)$$

$$\frac{m^*(\omega)}{m} = \frac{(\omega_p')^2}{4\pi} \frac{\sigma_2(\omega)}{|\hat{\sigma}(\omega)|^2} \frac{1}{\omega}. \qquad (17)$$

Due to causality,[48] $\Gamma_1(\omega)$ and $m^*(\omega)$ are related through the Kramers-Kronig integrals.[9] Such analysis allows us to look for interactions which would lead to energy dependent renormalization effects as the frequency dependent scattering rate and effective mass are related to the real and imaginary parts of the frequency dependent self-energy of the electrons.[49] Such analysis has been used before in studying the response of HF compounds[15,50,51] and high temperature superconductors.[52] In the lower frames of Fig. 6 the frequency dependence of the scattering rate $\Gamma_1(\omega)$ and of the effective mass $m^*(\omega)$ are displayed for different temperatures; for comparison we plot $\sigma_1(\omega)$ and $\epsilon_1(\omega)$ in Fig. 6a and b. As expected for a Drude metal, at $T > T^*$ the spectra of $\Gamma_1(\omega)$ and $m^*(\omega)$ are nearly frequency independent. As the temperature is lowered we observe a peak in the energy dependent scattering rate at the hybridization gap, as can be nicely

seen in the $T = 30$ K data of Fig. 6c. The existence of HF quasi-particles is confirmed by a low-frequency plasmon characterized by the zero-crossing in the spectra of the dielectric constant $\epsilon_1(\omega)$ shown in Fig. 6b. The decrease of $\Gamma_1(\omega)$ to lower frequencies corresponds to an increase of $m^*(\omega)$. At these intermediate temperatures, $T_N < T < T^*$, the effective mass m^*/m already reaches a value of 35.

The question remains how the optical response at very low frequencies can be described, i.e. for excitations of the zero-frequency mode; whether it is simply a renormalized Drude behavior. The Landau Fermi-liquid theory[53] predicts that the scattering rate due to electron–electron interactions in three dimensions should be quadratic both in temperature and frequency.[52–55] In order to examine the shape of the zero-frequency peak observed in the data, we have adopted the following phenomenological forms of $\Gamma_1(\omega)$ and $m^*(\omega)$, used by Sulewski *et al.* in their study of the Fermi liquid behavior of the heavy fermion compound UPt_3:[50]

$$\Gamma_1(\omega) = \Gamma_0 + \frac{\lambda_0 \alpha \omega^2}{1 + \alpha^2 \omega^2} \qquad (18)$$

and

$$\frac{m^*(\omega)}{m} = 1 + \frac{\lambda_0}{1 + \alpha^2 \omega^2}, \qquad (19)$$

where Γ_0 and λ_0 are the zero-frequency scattering rate and mass enhancement, respectively. $1/\alpha$ is a characteristic frequency (energy) of the process. These expressions obey the Kramers-Kronig relation and have the proper Fermi-liquid frequency dependence. The comparison of the low-frequency behavior of $\Gamma_1(\omega)$ at $T = 30$ K to the fit by Eq. (18) (inset of Fig. 6) confirms the main features: as the frequency increases, $\Gamma_1(\omega)$ grows and then saturates around 100 cm^{-1}. The present set of data, however, does not allow to conclude whether UPd_2Al_3 can be satisfactorily described within a Fermi-liquid formalism or not. These questions remain the subject of further investigations at lower frequencies.

The scattering rate drops more than one order of magnitude below 15 K. This can be explained by the freezing-out of spin-flip scattering below T_N. As was recently pointed out[56,57] in the context of high temperature superconductors, the energy dependent scattering rate is related to the electronic DOS. In fact, a sum-rule was suggested similar to Eq. (2). In the case of UPd_2Al_3 we can distinguish two gap structures with an enhanced DOS at the edges, as it is known from superconductors and low-dimensional semiconductors. Again, it would be of great interest to determine $\Gamma_1(\omega)$ of this narrow zero-frequency mode which remains in the AF state. Due to the influence of magnetic correlations it might be well distinct from the behavior at $T > T_N$ plotted in the inset of Fig. 6. The related experiments are currently in progress.

Decreasing the temperature below T_N results in a second peak of $\Gamma_1(\omega)$ and a strong increase of the effective mass around 1 cm^{-1}. Already seen at $T = 15$ K, this effect becomes stronger as the temperature is lowered to 2 K. The effective mass m^*/m levels off below this frequency and nicely matches the values obtained by thermodynamic methods[20,28] which are indicated by the point at $\omega = 0$ in Fig. 6d. Note, that due to the few data points, the features below 1 cm^{-1} are not significant; this range demands further studies. The important finding of our study is, that the magnetic ordering significantly changes the energy dependence $m^*(\omega)$: the strong increase of the effective mass does not occur at the hybridization gap at 10 meV, but mainly below the energy range which corresponds to the correlation gap at 0.2 meV. This infers that the magnetic correlations are of superior importance for the mass enhancement.

C. Spectral Weight

According to Eq. (2), the area under the conductivity spectrum is related to the density and the mass of the charge carriers. Well above the coherence temperature T^*, optical spectra of UPd_2Al_3 simply follow the Drude behavior of a normal metal with an unrenormalized plasma frequency of $\omega_p/(2\pi c) = 4.4 \cdot 10^4$ cm^{-1} as evaluated previously.[23] Assuming $m = m$, the free electron mass, we estimate a charge carrier density $n = 1.1 \cdot 10^{22}$ cm^{-3}. From experimental[32] and calculated[31] de Haas–van Alphen spectra we know that only approximately 35 % of the electrons contribute to the HF state; qualitatively we observe this fact also in our optical spectra. The plasma frequency which corresponds to those electrons (concentration n') which are affected by the formation of the HF state[58] is $\omega_p'/(2\pi c) = 9.5 \cdot 10^3$ cm^{-1}. Our analysis further infers that these carriers have a band mass $m' = 7m$. This also means, that a large fraction of the carriers is unaffected by the HF ground state and will not be considered in our further analysis.

Typical for a HF compound, below 100 cm^{-1} a narrow conductivity mode develops due to electronic correlations at lower temperatures. For $T > 20$ K but below T^*, the spectral weight of this contribution does not change significantly; the renormalized plasma frequency is $\omega_p^*/(2\pi c) \approx 4350$ cm^{-1}. A similar result of a temperature independent ω_p^* was obtained from our fit of the directly measured conductivity as displayed in the inset of the Fig. 4 by the open diamonds.

Assuming that the total number of charge carriers n' remains unchanged, sum-rule arguments give $\omega_p'/\omega_p^* = \sqrt{m^*/m'}$. Thus we obtain $m^*/m \approx 30$ which is in good agreement with the value obtained by thermodynamic methods of specific heat and susceptibility ($m^*/m = 41 - 66$)[20,28] and is somewhat smaller than the estimate from infrared measurements ($m^*/m = 85$).[23] Analyzing our data by the generalized Drude model (15), we have

obtained the energy dependence of the effective mass as plotted in Fig. 6d. For $T = 2$ K we find an enhancement of $m^*(\omega)/m = 45$, in excellent agreement with the above estimates of the spectral weight.

As the temperature decreases below T_N, a pseudogap develops in the optical spectra around 1.8 cm^{-1} (i.e. 0.2 meV) with important implications on the spectral weight. At low temperatures the optical weight consists of two contributions, the narrow $\omega = 0$ centered resonance and the charge carriers excited across the gap of energy $\hbar\omega_g$

$$\int_0^{\omega_c} \sigma_1(\omega)\,\mathrm{d}\omega = \int_0^{\omega_g} \sigma_1(\omega)\,\mathrm{d}\omega + \int_{\omega_g}^{\omega_c} \sigma_1(\omega)\,\mathrm{d}\omega. \quad (20)$$

Here we integrated up to a cut-off frequency $\omega_c/(2\pi c) \approx 100$ cm^{-1} which lies above the features associated to correlation effects but well below the interband transitions. The zero-frequency response contains only 10% of the overall spectral weight, the major contribution comes from the excitations across the gap. This agrees well with the above discussion of the peak in the DOS right above the gap. The temperature dependences of both components as well as their sum are presented in the inset of Fig. 4 (right axis). The contribution of the $\omega = 0$ response increases as the temperature decreases (open triangles in inset of Fig. 4); within our accuracy, this however, does not lead to a significant change of the overall spectral weight with temperature (open diamonds). The observed behavior can be taken as an indication that these two modes correspond to charge carriers localized at different parts of the Fermi surface. The coexistence of two different electronic subsystems in UPd$_2$Al$_3$ has also been suggested in Ref. 46.

The most interesting question is the relation between the AF ordering and the pseudogap origin. The fact that we also see the gap-like feature slightly above T_N up to 20 K or more does not rule out its connection to the magnetic ordering since an incommensurate phase was also observed up to $T \approx 20$ K by neutron diffraction experiments.[30]

IV. DISCUSSION

Since the development of the HF state in UPd$_2$Al$_3$ and the corresponding hybridization gap, which we observe around 100 cm^{-1}, was already discussed in Ref. 12,23 extensively, we concentrate now on the newly discovered feature at lower energies. Four possible explanations for the origin of the correlation gap at 0.2 meV will be considered: (i) the pseudogap in the optical response may be related to spin-wave excitations, (ii) the formation of a SDW ground state may lead to the opening of an energy gap, (iii) due to interaction the hybridization gap is shifted to low energies, and (iv) magnetic correlations in the AF ground state influence the electronic DOS spectra.

(i) From torque magnetization measurements Süllow et al.[59] found evidence of a gap in the spin-wave spectrum of the order of $E_g \approx 0.4$ meV, which is about the value of the pseudogap we see in the optical spectra. For $T > T_c = 2$ K inelastic neutron scattering experiments found a Lorentzian-shaped line around 1.5 meV which is ascribed to magnetic excitations.[29] Another gap observed at 0.4 meV was associated with superconductivity. All of these modes exhibit a strong temperature and $\mathbf{q}$-dependence.[29] Besides the resistivity $\rho(T)$ discussed above, the fall of $C(T)$ was also interpreted as the opening of a gap in the magnetic excitation spectrum.[20,46] Typically magnetic excitations, however, lead to a much smaller response in the optical properties. As it was shown above in Sec. III A, we were not able to obtain a reasonable fit of the observed features by a magnetic absorption process (cf. Fig. 2). Moreover, in our preliminary experiments in magnetic field[60] we have not seen any clear evidence in favor of the magnetic nature of the observed gap feature. We also think that the dielectric constant $\epsilon_1(\omega)$ would show a stronger influence of the magnetic field if the features were related to an AF resonance; in particular the frequency of the excitation would shift.

(ii) Below T_N a commensurate ordering of the rather large magnetic moments (0.85 μ_B) occurs in UPd$_2$Al$_3$;[30] also in the HF antiferromagnet URu$_2$Si$_2$ a commensurate structure develops but the ordered moment only amounts to 0.02 μ_B. Soon after the discovery of UPd$_2$Al$_3$ it was debated whether also in this compound the antiferromagnetic ordering is due to the SDW ground state like in URu$_2$Si$_2$. In contrast to URu$_2$Si$_2$, the resistivity of UPd$_2$Al$_3$ does not increase right below T_N, but the low temperature decrease can be well described by an activated behavior [Eq. (13)]. We do not think that the so-obtained gap value $E_g = 1.9$ meV indicates the formation of a SDW state[28,43]; it is much larger than the value obtained from our optical results (Fig. 4). The pseudogap feature we see in UPd$_2$Al$_3$ is not as clearly developed as the energy gap in URu$_2$Si$_2$ or UCu$_5$[21,23] and about a factor of five below the frequency one would expect from mean-field theory $E_g = 3.5 k_B T_N$. The opening of a SDW gap can be seen in the temperature dependent NMR relaxation rate of URu$_2$Si$_2$[61] yielding a reduction of the electronic density of states by a factor of three. A very similar behavior has been detected by ^{27}Al-NQR experiments[62] in UPd$_2$Al$_3$. Indications for a SDW behavior in isostructural UNi$_2$Al$_3$ have been reported by Y. Dalichaouch et al.[28] and by Uemura et al.[63] Recent ^{105}Pd-NMR and NQR experiments, however, speak against the SDW model for the UPd$_2$Al$_3$; the observed divergence in $1/T_1$ at T_N can be explained by a localized moment picture of uranium.[64]

(iii) Another possible mechanism of the pseudogap formation at these low energies is the change of the electronic DOS due to the coherence of screening conduction electrons in the Kondo lattice (so-called hybridization gap[3,11]). The coherence temperature T^* is usually

of the same order of magnitude as the single particle Kondo temperature T_K,[65] below which local moments are screened and a local Fermi-liquid picture applies. According to different experiments,[20,27,46] the coherence temperature of UPd_2Al_3 lies in the range from 20 K to 60 K, i.e. the hybridization gap should be approximately 1.9 to 5 meV. This is in excellent agreement with the 100 cm^{-1} gap (124 meV) we observe and hence assign to the hybridization gap following Eq. (4). However, there might be scenarios which also relate the low-frequency gap at 0.2 meV to the hybridization:

(a) The strong anisotropy in UPd_2Al_3 may lead to an anisotropic hybridization gap, and optical measurements see an "effective" value, which can be lower than the single-particle Kondo coupling energy. We want to recall a similar discussion for high-temperature superconductors where a complicated gap symmetry is made responsible for 'states in the gap' and a distinct optical response.[66–68] However, such a situation is only realized for f^1 or f^3 configurations of the U-ions, due to the absence of the Kondo screening for f^2 state. On the other side many experiments indicate U^{4+} oxidation state (f^2-configuration) in UPd_2Al_3,[69] but the electronic configuration of the U is not determined unambiguously.[26]

(b) By means of analytical and numerical calculations[70,71] the ratio T_K/T^* should be less than unity in case of a low density of screening electron (exhausting regime). It leads to a decrease of the coherence temperature T^*, which is a measure of the hybridization gap. In this case our Kondo-system would have single-particle excitations with an energy of the order $k_B T_K \approx$ 1.9 meV [it corresponds to the energy of the mode (1.5 meV), observed in the inelastic neutron scattering experiments[29]] and a collective resonance in the heavy particle assembly with about ten times lower energy. In favor of this hypothesis speaks the high magnetic moment of U (low concentration of the screening electrons) and also the fact that we observe the pseudogap up to $T \approx 20$ K: as the numerical calculations in the periodic Anderson model indicate, the Kondo resonance in the exhausting regime shows a much weaker temperature dependence and can be seen up to temperature $T \approx 10\,T^*$, in full agreement with our experimental observation.

(iv) The itinerant antiferromagnetism of a SDW is at odds with the formation of local moment magnetism deduced from susceptibility[20] and neutron scattering.[30] On the other hand, using self-consistent density functional calculations in the local approximation the magnetic structure and the size of the ordered moment of UPd_2Al_3 have been well described within a purely itinerant electron picture.[31] It was suggested[46] that two different electronic subsystems coexist in UPd_2Al_3. One of them is a rather localized uranium $5f$ state responsible for the magnetic properties, the other is delocalized and determines the heavy fermion and superconducting properties. From the London penetration depth[46] $\lambda_L(0)$=450 nm we calculate[72] the plasma frequency of the superconducting carriers $(2\pi\lambda_L(0))^{-1} = 3540$ cm^{-1} and find a good agreement with $\omega_p^*/(2\pi c) = 4350$ cm^{-1} obtained from the spectral weight of our low-frequency conductivity spectrum just above T_c (cf. inset of Fig.4). This has the following implications:

(a) In order to recover the spectral weight ρ^s of the δ-peak in the superconducting state (as determined from the penetration depth) according to the Tinkham-Ferrell sum rule,[9,72] we have to integrate the normal state conductivity $\sigma_1^n(\omega)$ up to a cut-off frequency $\omega_c^s/(2\pi c) = 100$ cm^{-1} (assuming that the conductivity decreases to zero up to this frequency) which is well above the frequency $2\Delta/(hc) = 4$ cm^{-1} at which the superconducting gap was observed by tunneling spectroscopy.[73] In conventional superconductors a change in the optical properties upon entering the superconducting state can be observed only up to approximately three times the gap frequency. A similar discrepancy of spectral weight was found in high-temperature superconductors[74] and gave argument to a change of the kinetic energy ΔK associated with the superconducting transition:[74,75]

$$\rho^s = \int_{0+}^{\omega_c^s} [\sigma_1^n(\omega) - \sigma_1^s(\omega)]\,\mathrm{d}\omega + \Delta K. \qquad (21)$$

Our results indicate that also for UPd_2Al_3 there is a loss of kinetic energy in the superconducting state. Since we were not yet able to probe the superconducting state and determine the superconducting gap by optical means,[76] we do not want to further speculate on the violation of the Tinkham-Ferrell sum rule and possible implications.

(b) All electrons seen in our low-energy spectra are in the HF ground state and eventually undergo the superconducting transition below T_c. We can definitely rule out an assignment of the gap to the localized carriers of the AF ordered states with the delocalized carriers contributing only to the narrow feature around $\omega = 0$ because with a plasma frequency of 1500 cm^{-1} at low temperatures, this feature contains only 18 % of the carriers which become superconducting. The small spectral weight below the correlation gap implies that the excitations above the gap stem from the delocalized states and that the pseudogap observed in our conductivity spectra is either inherent to the heavy-quasiparticle state or it is related to exchange correlations of the second subsystem.

Recently Sato et al.[77] argued that the magnetic excitations seen by neutron scattering produce effective interactions between itinerant electrons, and therefore are responsible for superconductivity. Similar conclusions where drawn from tunneling measurements on UPd_2Al_3 films.[73] Our results now indicate that already in the normal state electronic and magnetic excitations interact in the energy range which is relevant for superconductivity in UPd_2Al_3. From the frequency dependence of the effective mass $m^*(\omega)$ we can conclude that also the mass enhancement in the metallic state is strongly influenced by the magnetic correlations. Thus as magnetic excitons are supposed to be responsible for the superconductivity[73,77], we suggest that the localized magnetic excitations also

influence the properties of the normal state which were commonly assigned to the heavy-fermion ground state. We propose that the magnetic order in these compounds is the pre-requisite to the formation of the heavy quasi-particles and eventually of superconductivity.

It is expected that the *temperature dependence* of the quasiparticle formation, as observed in the enhancement of the effective mass, goes hand in hand with the *energy dependence* of the correlation effects, as probed by the f requency dependence of m^*; however, only very few experiments on heavy fermion systems have been performed in this regard.[50,51] From Fig. 6d we see a moderate enhancement of $m^*(\omega, T = 0)$ for frequencies below the hybridization gap and a larger one below the gap due to magnetic correlations. Accordingly, $m^*(\omega = 0, T)$ increases only slightly below T^* and shows a large enhancement below T_N. The latter behavior should also be observed in thermodynamic measurements of m^*.

V. OUTLOOK

If our explanation the optical properties of UPd_2Al_3 is valid, it may also apply to other heavy fermion compounds, in particular to UPt_3 which exhibits a similar behavior in many regards[2,17,78]. For UPt_3 the effective mass of the quasiparticles is larger ($m^*/m \approx 200$) and the relevant energy scales are lower. The coherence temperature $T^* \approx 30$ K, fluctuating short-range magnetic order occurs at $T_N = 5$ K,[79] and superconductivity sets in at $T_c = 0.5$ K.[17] Although the magnetic moment ($0.02\mu_B$) is much smaller, recent bandstructure calculations[80] infer the existence of localized as well as delocalized $5f$-electrons in UPt_3 very much similar to UPd_2Al_3. It was suggested that the observed enhancement of the quasiparticle mass results from the local exchange interaction of two localized $5f$-electrons with the remaining delocalized ones.

Millimeter wave experiments on UPt_3 crystals[18,50,81] which show a peak in the conductivity at 6 cm^{-1} for temperatures below 5 K indicate a similar scenario. We reanalyzed the optical properties of UPt_3 shown in Fig. 7a in the same way as described above (Sec. III B) and obtain similar features.[35] When the coherent ground state builds up ($T < T^*$), the optical conductivity increases for frequencies below 30 cm^{-1} (Fig. 7b). As the temperature drops below $T_N = 5$ K, magnetic ordering occurs and an energy gap progressively develops at about 3 cm^{-1} which is assigned to magnetic correlations.[18] In full analogy to the case of UPd_2Al_3, the frequency dependence of the effective mass of UPt_3 displayed in Fig. 7d clearly shows that only a marginal increase of m^* is observed around 30 cm^{-1}, while below the energies related to the magnetic correlations the mass is drastically enhanced. Thus for UPt_3 we also find that, as for UPd_2Al_3, the coupling of the localized and delocalized $5f$-electrons causes the heavy quasiparticles in UPt_3; these magnetic excitations are very likely to be responsible for superconductivity. More detailed electrodynamic studies on UPt_3 and on the superconducting state in general have to be performed since they seem to be the appropriate method to probe the energy dependence of the correlation effects which are the key issue for understanding the nature of the heavy quasiparticles. It remains to be seen how far our findings have implications on non-magnetic heavy fermions with a large effective mass. Of further interest would be the study of Ce compounds for which comparable band structure calculations do not yet exist.

VI. CONCLUSION

In conclusion, the electrodynamic response of UPd_2Al_3 in the low-energy range from 0.04 meV to 5 meV (0.33 cm^{-1} to 40 cm^{-1}) exhibits a behavior at low temperatures ($T \leq 20$ K) which cannot be explained within the simple picture of a renormalized Fermi liquid. At around 12 meV a hybridization gap develops below T^* which is characteristic for heavy fermions. The lower-frequency response shows the well-known renormalized behavior only above the magnetic ordering; below $T_N = 14$ K, however, additional features were discovered. Besides an extremely narrow (less than 1 cm^{-1}) zero-frequency response, we observe a pseudogap of about 0.22 meV. The experiments yield indications that this pseudogap is not a simple SDW gap or some excitation in the local magnetic moments system, but rather is connected to magnetic correlations on the delocalized charge carriers. We have argued, that this gap at extremely low energies is due to the influence of the localized magnetic moments on the itinerant electrons and this interaction is mainly responsible for the enhanced mass m^*. It appears that the formation of the heavy quasiparticles relies on the establishment of antiferromagnetic order rather than competition of the coherent singlet formation and the magnetic order.

---

* email: dressel@pi1.physik.uni-stuttgart.de

[†] Permanent address: General Physics Institute, Russian Academy of Sciences, Moscow, Russia

[‡] Present address: Max-Planck Institut für Metallforschung, Stuttgart, Germany; permanent address: Inst. Solid State and Semicond. Phys., Academy of Sciences of Belarus, Minsk, Belarus

[1] F. Steglich, J. Aarts, C. D. Bredl, W. Lieke, D. Meschede, W. Franz, and H. Schäfer, Phys. Rev. Lett. **43**, 1982 (1979).

[2] H.R. Ott, Prog. Low Temp. Phys. **11**, 215 (1987).

[3] N. Grewe and F. Steglich, in: Handbook on the Physics and Chemistry of Rare Earths, Vol. **14**, ed. by K.A. Gscheidner Jr. and L. Eyring (Elsevier, Amsterdam, 1991), p. 343.

[4] A.J. Millis and P.A. Lee, Phys. Rev. B **35**, 3394 (1987); A.J. Millis, M. Lavagna, and P.A. Lee, Phys. Rev. B **36**, 864 (1987)

[5] P. Coleman, Phys. Rev. Lett. **59**, 1026 (1987).

[6] A. Georges, G. Kotliar, W. Krauth, and M. J. Rozenberg, Rev. Mod. Phys. **68**, 13 (1996).

[7] P. Fulde, *Electron Correlations in Molecules and Solids*, 2nd ed. (Springer-Verlag, Berlin, 1993)

[8] A.C. Hewson, *The Kondo Problem to Heavy Fermions* (Cambridge University Press, Cambridge, 1997)

[9] M. Dressel and G. Grüner, *Electrodynamics of Solids* (Cambridge University Press, Cambridge, 2002).

[10] H. Fukuyama, in: *Theory of Heavy Fermions and Valence Fluctuations*, T. Kasuya and T. Saso, eds. (Springer-Verlag, Berlin, 1985).

[11] P. Wachter, Handbook on the Physics and Chemistry of Rare Earths, Vol. **19**, ed. by K.A.Gschneider Jr. and L. Eyring (North-Holland, Amsterdam 1994), p. 177.

[12] L. Degiorgi, Rev. Mod. Phys. **71**, 687 (1999).

[13] F. Marabelli and P. Wachter, Phys. Rev. B **42**, 3307 (1990).

[14] S. Bocelli, F. Marabelli, and E. Bauer, Physica B **199-200**, 34 (1994).

[15] S.V. Dordevic, D.N. Basov, N.R. Dilley, E.D. Bauer, and M.B. Maple, Phys. Rev. Lett. **86**, 684 (2001).

[16] L. Degiorgi, H.R. Ott, G. Grüner, M. Dressel, Z. Fisk, in: *Strongly Correlated Electronic Materials*, edited by K.S. Bedell et al. (Addison Wesley, Reading, 1994), p. 96; L. Degiorgi, S. Thieme, H.R. Ott, M. Dressel, G. Grüner, Y. Dalichaouch, M.B. Maple, Z. Fisk, C. Geibel, and F. Steglich, Z. Phys. B **102**, 367 (1997).

[17] G.R. Stewart, Rev. Mod. Phys. **56**, 755 (1984).

[18] S. Donovan, A. Schwartz, and G. Grüner, Phys. Rev. Lett. **79**, 1401 (1997).

[19] B. Maple, J. W. Chen, Y. Dalichaouch, T. Kohara, C. Rossel, M. S. Torikachvili, M. W. McElfresh, and J. D. Thompson, Phys. Rev. Lett **56**, 185 (1986); T.T.M. Palstra, A. A. Menovsky, and J. A. Mydosh, Phys. Rev. B **33**, 6527 (1986).

[20] C. Geibel, C. Schank, S. Thies, H. Kitazawa, C.D. Bredl, A. Böhm, M. Rau, A. Grauel, R. Caspary, R. Helfrich, U. Ahlheim, G. Weber, and F. Steglich , Z. Phys. B **84**, 1 (1991).

[21] D.A. Bonn, J.D. Garrett, and T. Timusk, Phys. Rev. Lett. **61**, 305 (1988).

[22] L. Degiorgi, H.R. Ott, M. Dressel, G. Grüner, and Z. Fisk, Europhys. Lett. **26**, 221 (1994).

[23] M. Dressel, L. Degiorgi, G. Grüner, P. Wachter, N. Sato, T. Komatsubara, and Y. Uemura, Physica B **199 & 200**, 173 (1994); L. Degiorgi, M. Dressel, G. Grüner, P. Wachter, N. Sato, and T. Komatsubara, Europhys. Lett. **25**, 311 (1994).

[24] An alternative explanation of the resistivity drop is based on the freezing out of the crystal field excitations.

[25] UPd_2Al_3 crystallizes in a hexagonal $PrNi_3Al_3$ structure[20].

[26] L. Paolasini, J.A. Paixao, and G.H. Lander, J. Phys.: Cond. Matter, **5**, 8905 (1993).

[27] C. Geibel, U. Ahlheim, C.D. Bredl, J. Diehl, A. Grauel, R. Helfrich, H. Kitazawa, R. Köhler, R. Modler, M. Lang, C. Schank, S. Thies, F. Steglich, N. Sato, and T. Komatsubara, Physica C **185 - 189**, 2651 (1991).

[28] Y. Dalichaouch, M.C. de Andrade, and M.B. Maple, Phys. Rev. B **46**, 8671 (1992).

[29] N. Sato, N. Aso, G.H. Lander, B. Roessli, T. Komatsubara, Y. Endoh, J. Phys. Soc. Jpn. **66**, 1884 (1997); N. Metoki, Y. Haga, Y. Koike, Y. Onuki, Phys. Rev. Lett. **80**, 5417 (1998); N. Bernhoeft, N. Sato, B. Roessli, N. Aso, A. Hiess, G.H. Lander, Y. Endoh, T. Komatsubara, Phys. Rev. Lett. **81**, 4244 (1998).

[30] A. Krimmel, P. Fischer, B. Roessli, H. Maletta, C. Geibel, C. Schank, A. Grauel, A. Loidl, and F. Steglich, Z. Phys. B **86**, 161 (1992); A. Krimmel, A Loidl, R Eccleston, C Geibel, and F Steglich, J. Phys.: Cond. Matter **8**, 1677 (1996).

[31] L.M. Sandratskii, J. Kübler, P. Zahn, and I. Mertig, Phys. Rev. B **50**, 15834 (1994); K. Knöpfle, A. Mavromaras, L.M. Sandratskii, and J. Kübler, J. Phys.: Cond. Matter **8**, 901 (1996).

[32] Y. Inada, H. Aono, A. Ishiguro, J. Kimura, N. Sato, A. Sawada, and T. Komatsubara, Physica B **199-200**, 119 (1994); Y. Inada, H. Aono, A. Ishiguro, J. Kimura, N. Sato, A. Sawada, T. Komatsubara, and H. Yamagami, Physica B **206-207**, 33 (1995); Y. Inada, H. Yamagami, Y. Haga, K. Sakurai, Y. Tokiwa, T. Honma, E. Yamamoto, Y. Onuki, and T. Yanagisawa, J. Phys. Soc. Jpn. **68**, 3643 (1999).

[33] M. Dressel, B.P. Gorshunov, A.V. Pronin, A.A. Mukhin, F. Mayr, A. Seeger, P. Lunkenheimer, A. Loidl, M. Jourdan, M. Huth, H. Adrian, Physica B **244**, 125 (1998)

[34] M. Dressel, B.P. Gorshunov, N. Kasper, B. Nebendahl, M. Huth, H. Adrian, J. Phys.: Cond. Matter **12** L633 (2000)

[35] M. Dressel, N. Kasper, K. Petukhov, B. Gorshunov, G. Grüner, M. Huth, and H. Adrian, Phys. Rev. Lett. *(in press)*, cond-mat/0201167.

[36] M. Huth, A. Kaldowski, J. Hessert, Th. Steinborn, and H. Adrian, Solid State Commun. **87**, 1133 (1993); M. Huth, A. Kaldowski, J. Hessert, C. Heske, and H. Adrian, Physica B **199 & 200**, 116 (1994).

[37] A.A. Volkov, Yu. G. Goncharov, G.V. Kozlov, S.P. Lebedev, and A.M. Prokhorov, Infrared Phys. **25**, 369 (1985); A.A. Volkov, G.V. Kozlov, and A.M. Prokhorov, Infrared Phys. **29**, 747 (1989).

[38] O. Klein, S. Donovan, M. Dressel, and G. Grüner, Int. J. Infrared and Millimeter Waves **14**, 2423 (1993).

[39] S. Donovan, O. Klein, M. Dressel, K. Holczer, and G. Grüner, Int. J. Infrared and Millimeter Waves **14**, 2459 (1993).

[40] M. Dressel, S. Donovan, O. Klein, and G. Grüner, Int. J. Infrared and Millimeter Waves **14**, 2489 (1993).

[41] D.N. Peligrad, B. Nebendahl, C. Kessler, M. Mehring, A. Duli, M. Paek, and D. Paar, Phys. Rev. B **58**, 11652 (1998).

[42] N. H. Andersen, in *Crystalline Electric Field and Structural Effects in f-Electron Systems*, ed. by J.E. Crow, R.P. Guertin, and T.W. Mihalisin (Plenum, New York, 1970), p. 173.

[43] K. Bakker, A. de Visser, L.T. Tai, A.A. Menovsky, and J.J.M. Franse, Solid State Commun. **86**, 497 (1993).

[44] J. Aarts, A.P. Volodin, A.A. Menovsky, G.J. Nieuwenhuys, and J.A. Mydosh, Europhys. Lett. **26**, 203 (1994).

[45] M. Huth, M. Jourdan, and H. Adrian, Physcia B **281 & 282**, 882 (2000)

[46] R. Caspary, P. Hellmann, M. Keller, G. Sparn, C. Wassilew, R. Köhler, C. Geibel, C. Schank, and F. Steglich, Phys. Rev. Lett. **71**, 2146 (1993); R. Feyerherm, A. Amato, F. N. Gygax, A. Schenck, C. Geibel, F. Steglich, N. Sato, and T. Komatsubara, Phys. Rev. Lett. **73**, 1849 (1994).

[47] P.Y. Yu and M. Cardona, *Fundamentals of Semiconductors* (Springer-Verlag, Berlin, 1996).

[48] J. W. Allen and J. C. Mikkelsen, Phys. Rev. B **15**, 2952 (1977).

[49] A.A. Abrikosov, L.P. Gor'kov, and I.Ye Dzyaloshinskii *Quantum field theoretical methods in statistical physics* (Pergamon, New York, 1965).

[50] P. E. Sulewski, A. J. Sievers, M. B. Maple, M. S. Torikachvili, J. L. Smith, and Z. Fisk, Phys. Rev. B **38**, 5338 (1988).

[51] A.M. Awasthi, L. Degiorgi, G. Grüner, Y. Dalichaouch, and M.B. Maple, Phys. Rev. B **48**, 10692 (1993)

[52] J. Ruvalds and A. Virosztek, Phys. Rev. B **43**, 5498 (1991).

[53] D. Pines and P. Nozières, *The Theory of Quantum Liquids* (Benjamin, New York, 1966).

[54] N.W. Ashcroft and N.D. Mermin, *Solid State Physics* (Holt, Rinehart and Winston, New York, 1976)

[55] R. N. Gurzhi, Sov. Phys. JETP **8**, 673 (1959).

[56] F. Marsiglio, J.P. Carbotte and E. Schachinger, Phys. Rev. B **65**, 014515 (2002).

[57] D.N. Basov, E.J. Singley, and S.V. Dordevic, Phys. Rev. B **65**, 054516 (2002).

[58] The evaluation of effective charge carriers was done by using the relation: $(\omega'_p)^2 = (\omega^*_p)^2\big|_{2K} + 8\left[\int \sigma_1(\omega)\,d\omega\big|_{300K} - \int \sigma_1(\omega)\,d\omega\big|_{2K}\right]$.

[59] S. Süllow, B. Janossy, G.L.E. van Vliet, G.J. Nieuwenhuys, A.A. Menovsky, and J.A. Mydosh, J. Phys.: Condens. Matter **8**, 729 (1996).

[60] N. Kasper, B. Gorshunov, D.N. Peligrad, M. Dressel, M. Huth, and H. Adrian (*unpublished*).

[61] T. Kohara, Y. Kohori, K. Asayama, Y. Kitaoka, M.B. Maple, and M.S. Torikachvili, Solid State Commun. **59**, 603 (1986).

[62] H. Tou, Y. Kitaoka, K. Asayama, C. Geibel, C. Schank, and F. Steglich, J. Phys. Soc. Jpn. **64**, 725 (1995).

[63] Y.J. Uemura and G.M. Luke, Physica B **186-188**, 223 (1993).

[64] K. Matsuda, Y. Kohori, and T. Kohara, Phys. Rev. B **55**, 15 223 (1997).

[65] G. Grüner and A. Zawadowski, Rep. Prog. Phys. **37**, 1497 (1974); *id.*, in: *Progress in Low Temperature Physics, Vol. VII B*, edited by D. F. Brewer (North-Holland, Amsterdam, 1978), p. 591.

[66] M.J. Graf, M. Palumbo, D. Rainer, and J.A. Sauls, Phys. Rev. B **52**, 10588 (1995).

[67] S. M. Quinlan, P.J. Hirschfeld, and D. J. Scalapino, Phys. Rev. B **53**, 8575 (1996).

[68] I. Schuerrer, E. Schachinger, and J.P. Carbotte, Physica C, **303**, 287 (1998).

[69] F. Steglich, U. Ahlheim, A. Böhm, C.D. Bredl, R. Caspary, C. Geibel, A. Grauel, R. Helfrich, R. Köhler, M. Lang, A. Mehner, R. Modler, C. Schank, C. Wassilew, G. Weber, W. Assmus, N. Sato, and T. Komatsubara, Physica C, **185-189**, 379 (1991); A. Grauel, A. Böhm, H. Fischer, C. Geibel, R. Köhler, R. Modler, C. Schank, F. Steglich, G. Weber, T. Komatsubara, and N. Sato, Phys. Rev. B **46**, 5818 (1992).

[70] S. Burdin, A. Georges, and D. R. Grempel, Phys. Rev. Lett. **85**, 1048 (2000).

[71] A.N. Tahvildar-Zadeh, M. Jarrell, and J. K. Freericks, Phys. Rev. Lett. **80**, 5168 (1998).

[72] M. Tinkham *Introduction to Superconductivity* 2nd ed. (New York:McGraw Hill,1996).

[73] M. Jourdan, M. Huth, and H. Adrian, Nature **398**, 47 (1999).

[74] D.N. Basov, S.I. Woods, A.S. Katz, E.J. Singley, R.C. Dynes, M. Xu, D.G. Hinks, C.C. Homes, and M. Strongin, Science **283**, 49 (1999); D.N. Basov, C.C. Homes, E.J. Singley, M. Strongin, T. Timusk, G. Blumberg, and D. van der Marel, Phys. Rev. B **63**, 134514 (2001).

[75] J.E. Hirsch, Physica C **199**, 305 (1992).

[76] D.N. Basov, *private communication*

[77] N.K. Sato, N. Aso,m K. Miyake, R. Shiina, P. Thalmeier, G. Varelogiannis, C. Geibel, F. Steglich, P. Fulde, and T. Komatsubara, Nature **410**, 340 (2001).

[78] Z. Fisk, D.W. Hess, C.J. Pethick, D. Pines, J.L. Smith, J.D. Thompson, and J.O. Willis, *Science* **239**, 33-42 (1988).

[79] J.K. Kjems and C. Broholm, J. Mag. Magn. Mater. **76**, 371 (1988).

[80] G. Zwicknagl, A.N. Yaresko, and P. Fulde, Phys. Rev. B **65**, 081103 (2002).

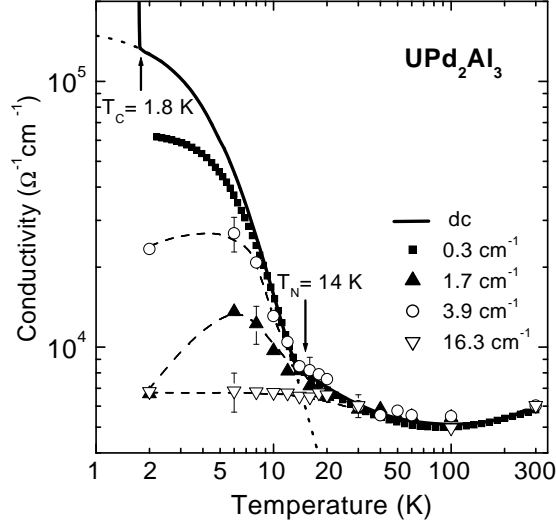[81] F. Marabelli, G. Travaglini, P. Wachter, J.J. Franse, Solid State Commun. **59**, 381 (1986).

FIG. 1. Temperature dependence of the dc conductivity of the UPd$_2$Al$_3$ film together with the ac conductivities obtained at different frequencies as indicated. The dotted line represents a fit of the dc conductivity using Eq. (13) with the gap $E'_g = 1.9$ meV. The dashed lines are guides to the eye; note the non-monotonous frequency dependence at low temperatures.
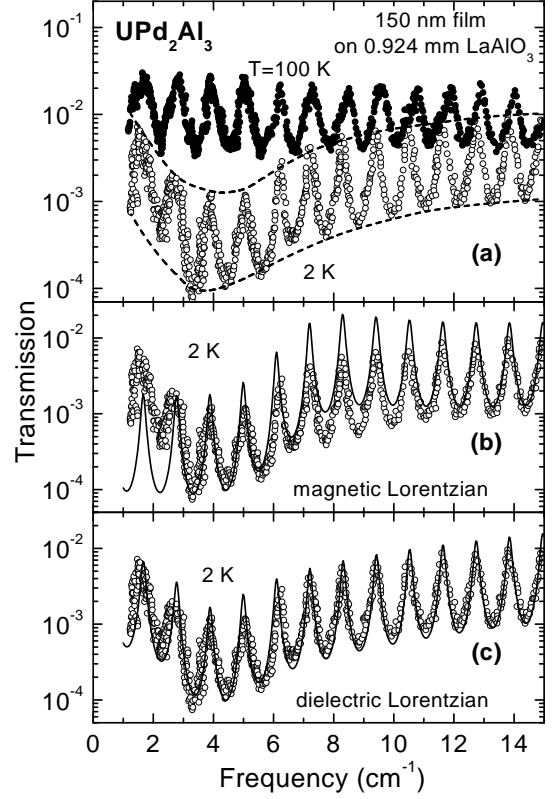

FIG. 2. Transmission spectra $T_F(\omega)$ of a 150 nm thick UPd$_2$Al$_3$ film on LaAlO$_3$ (thickness 0.924 mm) for temperatures $T = 100$ K and 2 K (a); the dashed lines connecting minima and maxima (due to multi-reflection within the substrate) are drawn to emphasize the overall frequency dependence of the transmission of the film. The middle (b) and the bottom (c) panels present the fits of the transmission spectra for $T = 2$ K using the models of 'magnetic' and 'dielectric' oscillators (Lorentzians), respectively; the oscillator parameters are given in the text.
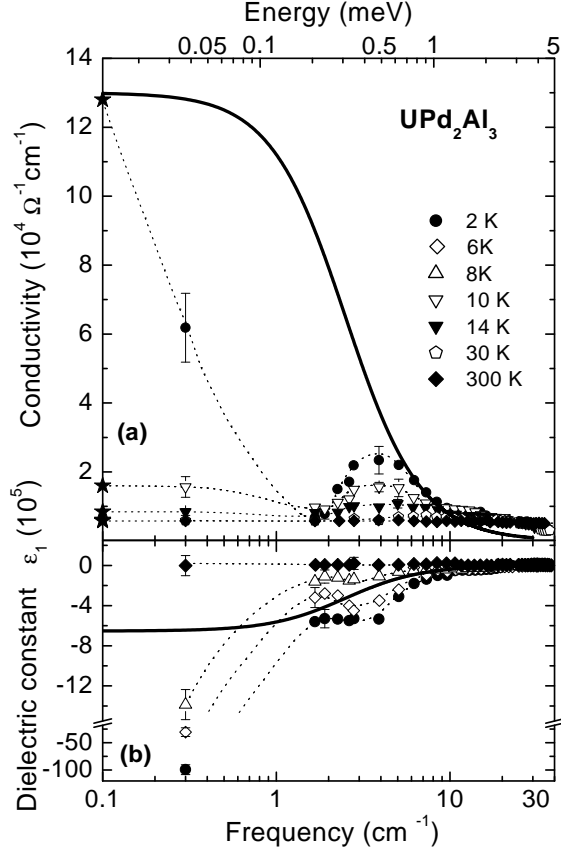
FIG. 3. The low-frequency optical conductivity (a) and the dielectric constant (b) of UPd$_2$Al$_3$ as a function of frequency at several temperatures. The dc conductivity is shown by the stars on the left axis of the upper panel. The dashed lines are drawn to guide the eye. The solid lines correspond to the renormalized Drude behavior [Eq. (3)] assuming $\sigma_{dc} = 1.25 \cdot 10^5 (\Omega \text{cm})^{-1}$ and $\Gamma^*/(2\pi c) = 2.5$ cm^{-1}.
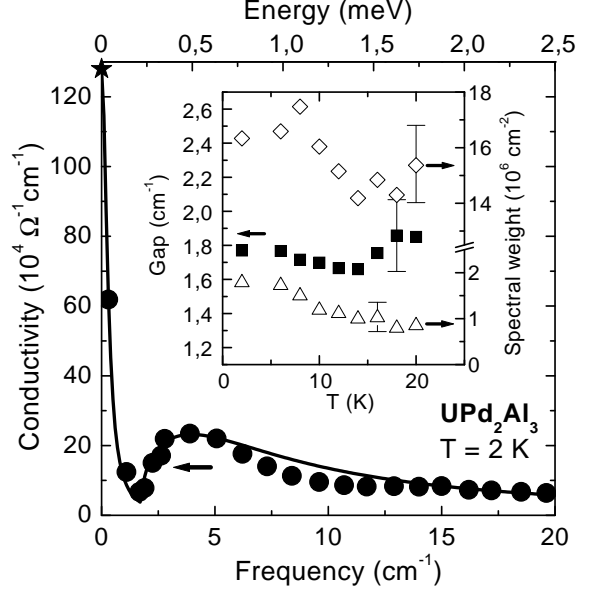
FIG. 4. Optical conductivity $\sigma_1(\omega)$ of UPd$_2$Al$_3$ at $T = 2$ K. The line corresponds to the fit by Eq. (14). In the inset the temperature dependences of the gap frequency (full squares, left axis) obtained from the fit is displayed. Also shown is the spectral weight of the $\omega = 0$ resonance (open triangle, right axis) and of all the excitations above and below the gap (open diamonds, right axis). For details see text.
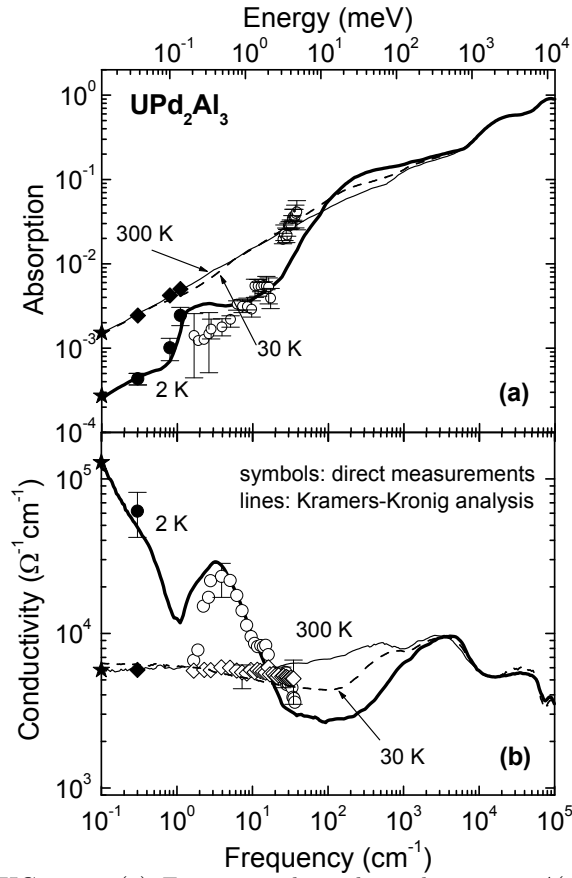
13

FIG. 5.   (a) Frequency dependent absorption $A(\omega)$ of UPd$_2$Al$_3$ at different temperatures shown over a wide frequency range. The solid stars on the left axis represent the dc values in a Hagen-Rubens behavior (10); the full symbols in the microwave range are obtained by cavity perturbation technique; the open symbols present absorption evaluated from the transmission and phase measurements by the Mach-Zehnder interferometer (only 2 K data are plotted for clarity reasons). The lines are obtained by combining the various optical investigations (transmission through films and reflection of bulk samples) and simultaneously matching the directly measured conductivity and dielectric constant. (b) Optical conductivity of UPd$_2$Al$_3$ as evaluated by a Kramers-Kronig analysis of the above absorptivity data. The stars on the left axis indicate the dc conductivity; the full points were obtained by the 10 GHz cavity method. The open symbols correspond to the direct determination of the optical conductivity using the transmission and the phase shift obtained by the Mach-Zehnder interferometer.
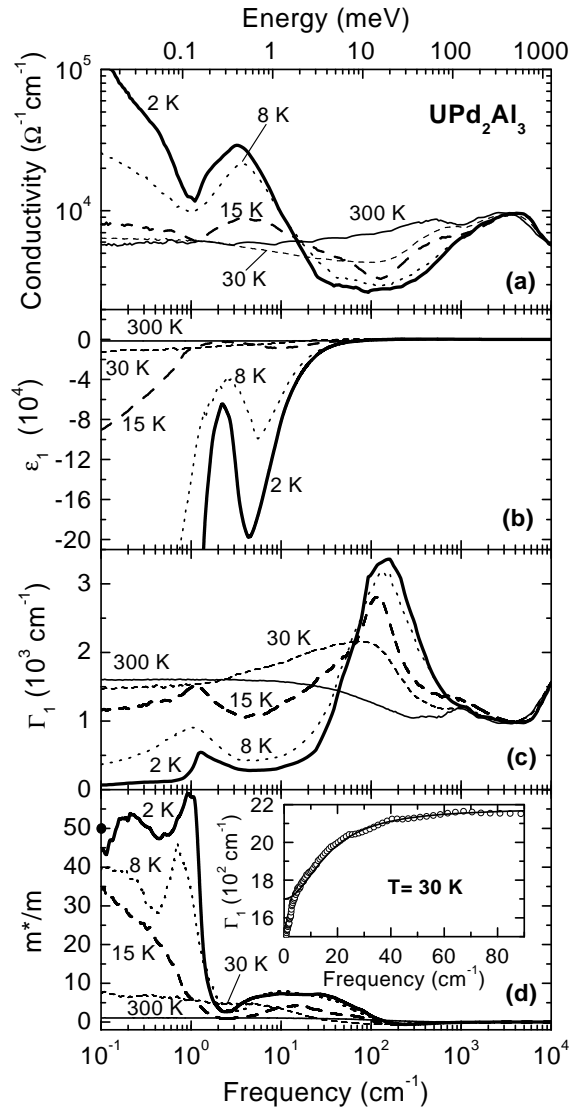
FIG. 6. Frequency dependence of (a) the optical conductivity $\sigma_1(\omega)$, (b) the dielectric constant $\epsilon_1(\omega)$, (c) the scattering rate $\Gamma_1(\omega)$, and (d) the effective mass $m^*(\omega)/m$ of UPd$_2$Al$_3$ for different temperatures. The point on the left axis of panel (d) corresponds to the effective mass determined by thermodynamic measurements (data from Refs. 20,28), and the inset shows the comparison of $\Gamma_1(\omega)$ at $T = 30$ K with the behavior (18) expected for Landau's theory of a Fermi-liquid.
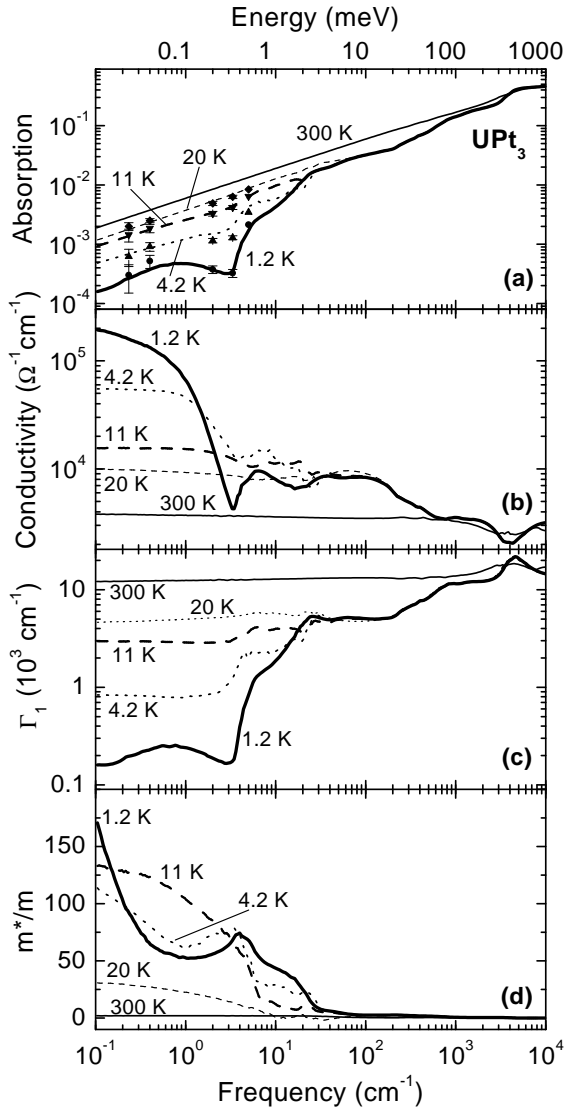
FIG. 7. Frequency dependence of (a) the absorption $A(\omega)$, (b) the optical conductivity $\sigma_1(\omega)$, (c) the scattering rate $\Gamma_1(\omega)$, and (d) the effective mass $m^*(\omega)$ of UPt$_3$ for different temperatures. The absorption data are calculated form the experimental results of Refs. 18,50,81.